Compressive Strength of Solid Clay Brick Masonry under Eccentric Loading

by

A. BRENCICH[1], C. CORRADI[1], L. GAMBAROTTA[1], G. MANTEGAZZA[2], E. STERPI[1]
[1]*Department of Structural and Geotechnical Engineering – University of Genoa – Italy*
[2]*RUREDIL s.p.a. - Milan - Italy*

ABSTRACT
Arches, vaults and pillars generally experience eccentric normal force. As a consequence, the classical theories of masonry collapse, developed for concentrically compressed brickwork, are not directly applicable. In this paper experimental data on solid clay brick and lime-mortar masonry prisms, eccentrically loaded, are presented. Comparing the results to the response of a FEM model, some hints on the collapse mechanism of masonry show that the edge effects greatly affect the load carrying capacity of the brickwork. Besides, the plane section assumption is found to be acceptable up to the ultimate compressive strength, allowing relatively simple models to be used for arch-type structures.

1. INTRODUCTION

In many technical applications, mainly load bearing walls, masonry experiences a substantially concentric loading; the stress state, which is inhomogeneous because of the intrinsic structure of brickwork, may be described by the mean value of the local stress field. In these cases, masonry can be modelled as an homogeneous brittle material and the classical structural mechanics for continuum materials is applicable. In order to evaluate the load carrying capacity of the structure, failure criteria are derived from quasi-brittle materials modified either on experimental grounds or on theoretical work. This approach is suitable when the intrinsic anisotropy and periodicity of masonry can be averaged to macroscopic equivalent mechanical parameters and failure criteria, i.e. for veneer walls, masonry panels and their assemblages, and full buildings. When addressing masonry pillars, arches or vaults, which experience eccentric normal forces, the evaluation of the compressive strength from the properties of the different materials does not seem to have been investigated, while the experimental and theoretical research on uniformly compressed masonry cannot be directly extended to this stress state.

Over the last decades research has concentrated on deformation and failure theories for compressed masonry and on the experimental testing of brickwork, both with the aim of setting up some empirical failure criterion and of defining the parameters of a mechanical model [1, 2].

A common hypothesis based on some experimental evidence is that the mortar/brick interface does not experience sliding under concentric compressive stress states. Starting from this observation, many failure theories in compression have been proposed most of which assume that masonry can be modelled as a layered unlimited continuum. The compatibility conditions at the mortar/brick interface lead to a tri-axial compressive stress state in the mortar and a tri-axial tensile-tensile-compressive one in the brick, Figure 1, so that the brickwork collapse mechanism is that of vertical cracking of bricks. Being this masonry model an unlimited layered continuum, the stresses are assumed uniform through both the brick and the mortar thickness. Collapse takes place when the tensile stress in the brick, calculated assuming linear [3] and non-linear [4, 5] elastic relationships, attains its compressive-tensile-tensile strength. Other theories rely on a limit analysis approach [6] or on a limit strain condition [7] allowing more sophisticated failure criteria that turn out to be in reasonable agreement with the measured uniform compressive strength [5, 8].

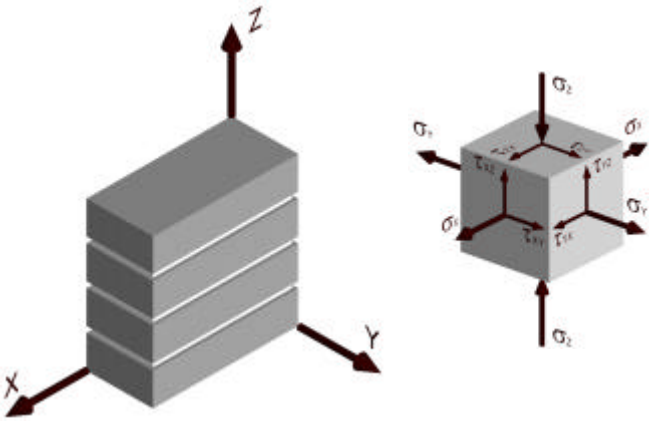

Figure 1 – Triaxial stress state in the brick and in the mortar

The simplest mechanical model that can be formulated for masonry retains the assumption of an homogenous equivalent material and needs, at least, the compressive strength and an equivalent elastic modulus to be given. Only few experimental data on eccentric loading are available [9, 10], mainly focused in defining the load carrying capacity of the structural brickwork; poor detailing is given on the effective collapse mechanism. The only detailed tests [11] refer to stone unit dry assemblages; the absence of the mortar joints makes these data not very useful for solid clay brickwork. For this reason, a careful investigation on masonry strength and collapse mechanisms under non-uniform stresses is needed. The present work is a step for setting up an adequate testing procedure of solid clay brick masonry prisms and a first glance in the collapse mechanism of brickwork under eccentric loading.

In order to evaluate the effect of the load eccentricity on the masonry resistance and collapse mechanisms, and with the aim of extending the classical approach to masonry collapse, a series of experimental tests have been performed on short prisms of 5.5x11x24 cm solid clay bricks and 1:1:5 cement-lime mortar, intended to represent a typical brickwork. The eccentric loading reproduces the stress distribution typical of an arch, while symmetry conditions allow the prism to represent a generic section of an arch, a vault or a pillar. The prisms are 24 cm large, 11 cm thick and 27 cm high, reproducing mainly thin structures; the load eccentricity ranges from 0 to 5/12 of the section height so that moderately to highly non uniform compressive stresses have been investigated.

The results of the experimental tests are compared to FEM analyses along with the theoretical and experimental collapse mechanisms of the brickwork. Some comparisons with other mechanical models, assuming masonry as an unlimited layered continuum, are carried out.

2. TESTING PROCEDURE

The masonry prism consist of a stack of four 5.5x11x24 cm bricks and five 10 mm thick mortar joints of 60 days of age; the global height of the stack is therefore 270 mm. The upper and lower mortar joints are in direct contact with the steel plates of the testing machine.

The testing setup is represented in Figure 2; minor details are omitted for the sake of simplicity. The load measuring device is a C5 class *HBM-RTN* load cell with a 0.01% precision and is located in-between the upper plate and the testing machine. The upper and lower plates are connected through cylindrical hinges that allow the load line to be precisely identified. The relative displacements are measured by means of mechanical devices with a 0.01mm precision (0.001 mm precision for testing the materials).

The displacement of the upper part of the machine is controlled and locked by means of a mechanical device; the displacements between the specimen ends are measured in three different points directly on the plates (bases 1, 2 and 3) in order to quantify the absolute relative displacement of the steel plates and their relative rotation. Six sections are used to control the position of the central joint, two at the extremities (4 and 9) and two on each side of the specimen at $1/4^{th}$ and $3/4^{th}$ of the brick length (5 and 6 on one side, 7 and 8 on the other one). The devices had been connected to the specimen by means of screw bolts glued with epoxy resins in the external part of the brick, Figure 3.

The moving end of the machine is displacement controlled, while the load is measured thorough the load cell. In this way, the load process is substantially a displacement-controlled procedure. The load cell can be considered as a spring with high stiffness; up to the limit load this does not affect the results at all; it significantly alters the measurements only far after the material collapse, at a point when the softening curve has already lost any mechanical meaning.

Some of the material mechanical properties have been measured in direct compression tests, according to EN196 standard, under displacement controlled loading and by means of a testing setup similar to that of Figure 2 but for the load cell (50 kN C5 class AEP-TCE cell with a 0.01% precision) and the overall dimensions.

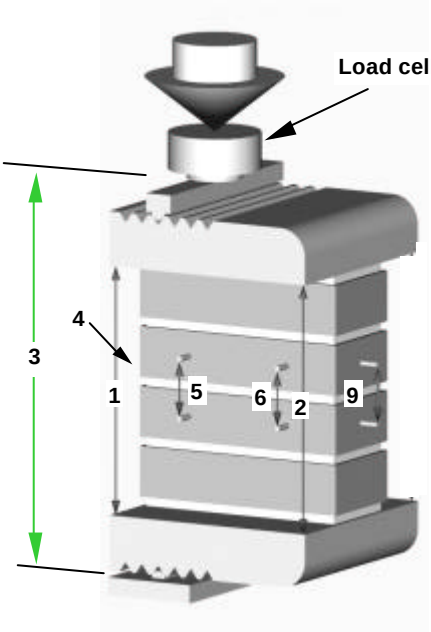

Figure 2 – Testing setup

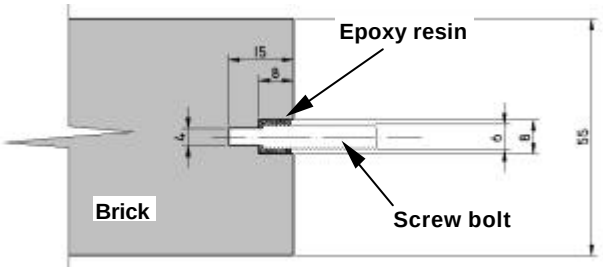

Figure 3 – Connection of the measuring devices to the brick

Table 1
Mechanical parameters for brick and mortar
(experimental data and assumptions)

BRICK		
Property	**Value**	**Notes**
E_b [N/mm^2]	2400±200	Direct compression average on 3 specimens
ν_b	0.05±0.007	Direct compression average on 3 specimens
f_t [N/mm^2]	3.4±0.25	TPB - average on 3 specimens
f_c [N/mm^2]	18.7±2.1	Direct compression average on 6 specimens
MORTAR		
E_m [N/mm^2]	335	see text
ν_m	0.2	Rots [15]
f_t [N/mm^2]	1.4	Brencich et al. [16] – see text
f_c [N/mm^2]	14.7±0.6	Direct compression average on 6 specimens

The elastic modulus of the brick was found to be quite low, but the measured figure fits well other experimental data on these materials [12] showing that clay brick units can exhibit unexpectedly low elastic moduli.

Even though the 1:1:5 cement-lime mortar was intended to

represent a typical European mortar with low compressive strength, the experimental outcome showed a very high strength in compression. The elastic modulus of the masonry assemblage under concentric loading (12300 N/mm^2) fits reasonably well with some laboratory [13] and other *in-situ* tests on Italian historical railway bridges [14]. The tensile strength for brick of table 1 is the average over three TPB tests.

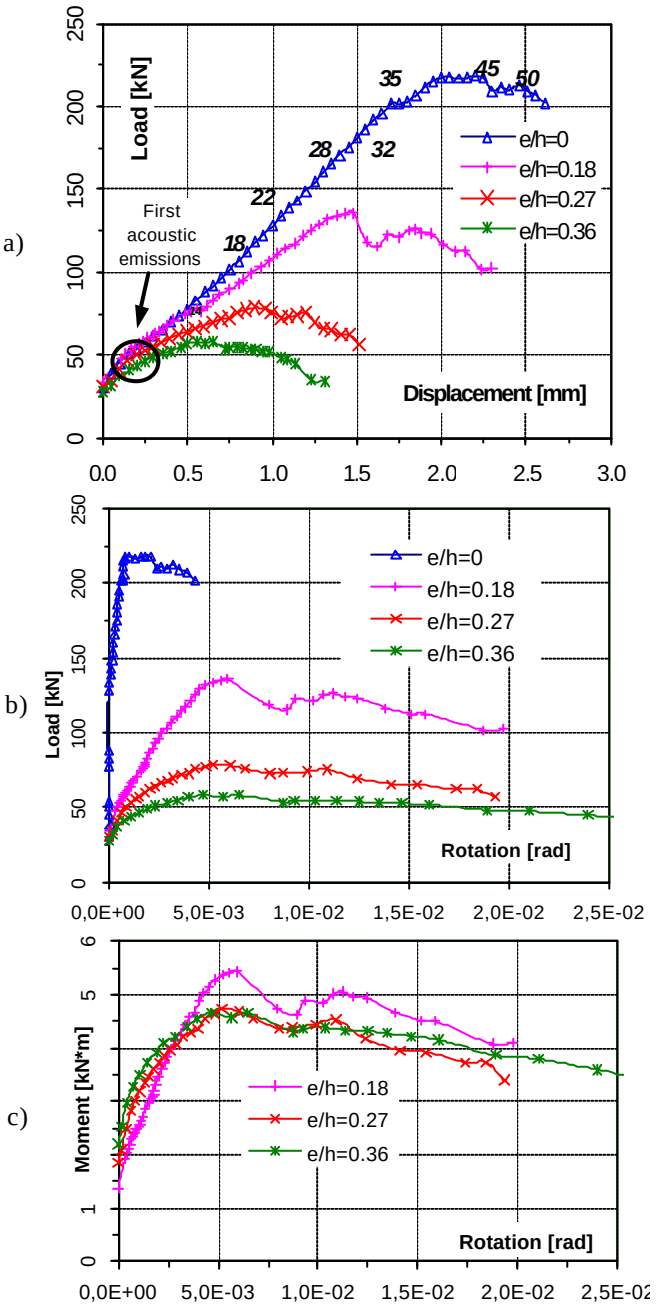

Figure 4 – a) Load-Displacement, b) Load-Rotation and c) Moment-Rotation curves

Mortar specimen are manufactured and cured in different conditions from those affecting the mortar joints. Adequate vibration makes the mortar prisms to incorporate much less air than the joints; besides, being manufactured in steel boxes, they do not suffer from variations in water content as, on the contrary, happens for the mortar at direct contact with the brick.

The elastic modulus and the Poisson's ratio are global properties which are quite difficult to evaluate on the small specimen used to test the compressive strength of mortars. For these reasons, some of the mechanical values could not be measured and had to be assumed from literature.

The Poisson's ratio has been deduced from literature [15], while the tensile strength was defined according to well established data [16]. The elastic modulus of mortar was assumed in such a way to reproduce the global elastic modulus of masonry. In the elastic part of the response, under plane strain conditions, the equivalent modulus for masonry E_M can be calculated as a function of the mechanical parameters of the different materials [3]:

$$\frac{1}{E_M} = \frac{h_b}{E_b} + \frac{h_m}{E_m} + \\ +2h_m h_b \frac{n_b E_m - n_m E_b}{h_m(1-n_b)\ E_m + h_b(1-n_m)E_b}\left(\frac{n_m}{E_m^2} - \frac{n_b}{E_b^2}\right), \quad (1)$$

where $h_m = t_m/(t_m + t_b)$, $h_b = t_b/(t_m + t_b)$ are the volume fractions of mortar and brick and t_m and t_b are the respective thickness. Eq. (1) is essentially a combination rule of the two distinct phases; a third term couples mortar and brick properties but contributes for less than 1% to the global elastic modulus. In this way eq. (1) turns out to be quite insensitive to the values of the Poisson's ratio.

Once the mechanical parameters for brick and Poisson's ratio of the mortar are given, the elastic modulus for mortar has been assumed so as to reproduce the global modulus for masonry deduced from the experimental tests. The mechanical parameters are given in table 1.

3. TEST RESULTS

Five different eccentricities have been tested: e/h = 0, 0.18, 0.27, 0.36, 0.45. The latter one gave uncertain results since the limit load was close to the load cell minimum allowable measurement and the displacement was so small to be close to the testing apparatus precision; in this case only the ultimate load and displacement were recorded. For each of the other eccentricities load-displacement, load-rotation and moment-rotation curves have been recorded, Figure 4. For e/h=0 (concentric loading) no significant rotation was found, as it should, up to the limit load point. The softening phase is quite long; the last point simply marks the end of the meaningful part of the test and does not stand for the sudden collapse of the specimen. The circle marks the point at which acoustic emission was detected, showing the beginning of internal crack propagation. Both the tests with the whole section compressed (e/h = 0 and e/h = 0.18) show a significantly linear initial response; on the other hand, under highly eccentric loading conditions the non-linear response is evident.

The relative displacements of the bases 4 to 9 have been recorded throughout the test and are represented in Figure 5 for the eccentric loading. The 100% curves stand for the position of the central joint at the displacement corresponding to the limit load; figures lower than 100% indicate the position of the joint at that percentage of the displacement at collapse, whilst over 100% indicate the joint position in the softening phase. It can be seen that there are hints for corroborating the hypothesis that the cross

section remains plane up to the peak load. Once the limit point is reached, the compressed part of the section crashes, but the other part of the section remains plane, at least on the average.

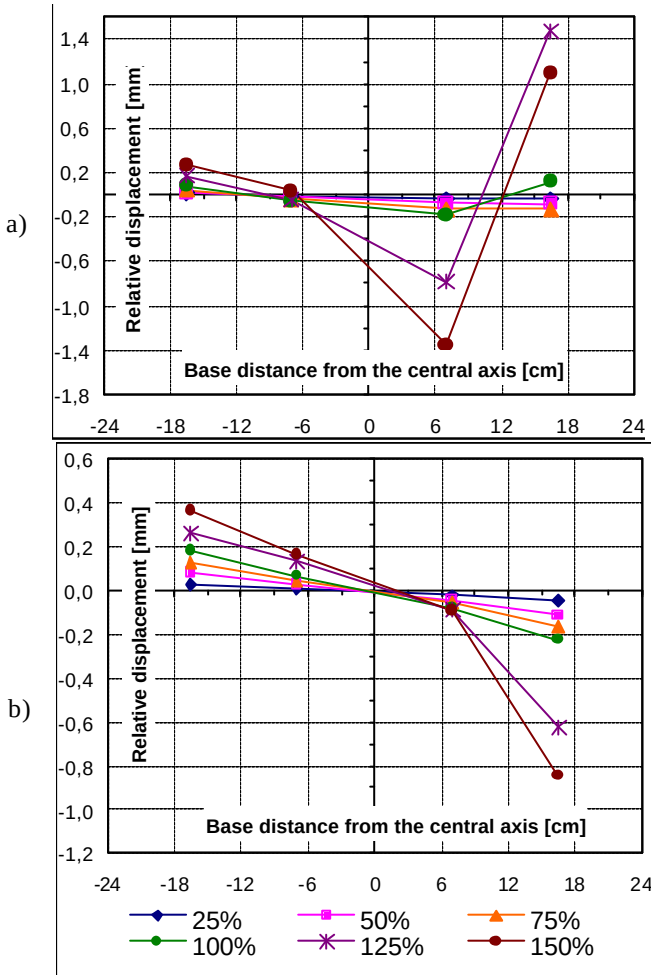

Figure 5 – Position of the central joint for a) *e/h*=0.18 and b) *e/h*=0.36

Whilst in Figure 6 a typical crack pattern is shown (numbers refer to the load step at which the crack appeared), Figures 7 and 8 show photos of the specimen at the end of the test before and after removal of the outside parts. The H-shaped crack pattern of Figure 7 enlightens the lateral instability of a thin sheet of brick; in Figure 8 this thin sheet has been removed (right bottom hand side) showing that a crack almost parallel to the surface had developed. Many other cracks indicate that such a phenomenon takes place also in the central bricks. The inner core seems to be less damaged than the external parts of the brick. Cracks extend to the mortar joint only when some parts of the brick tend to detach.

It has to be noted that the measuring devices and their connections to the prisms were never found to activate cracking. In fact, also till the final stage of collapse, neither a screw bolt originated any crack.

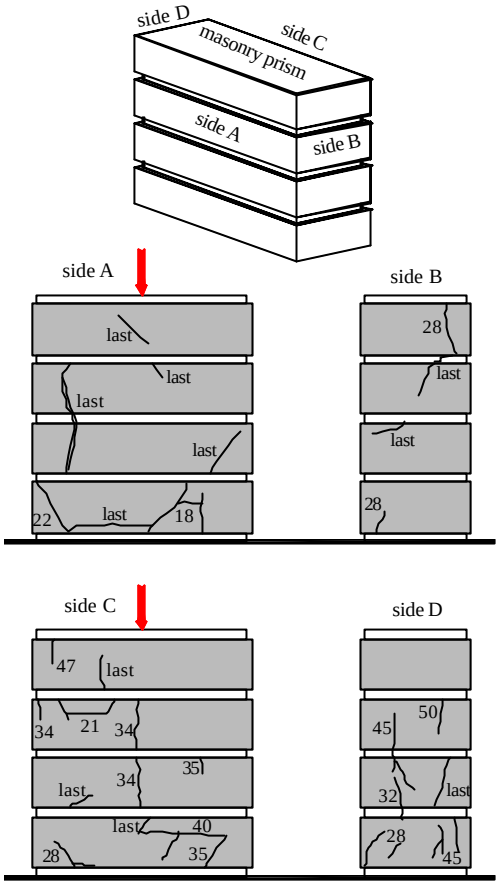

Figure 6 – Crack pattern evolution for concentric loading – the numbers indicate the load step at which the crack was detected

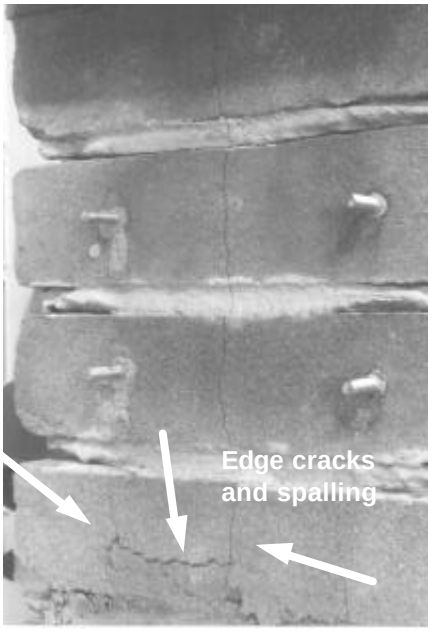

Figure 7 – Concentric loading – side C bottom: spalling of the outside part of the brick. White arrows indicate the typical H-shape pattern

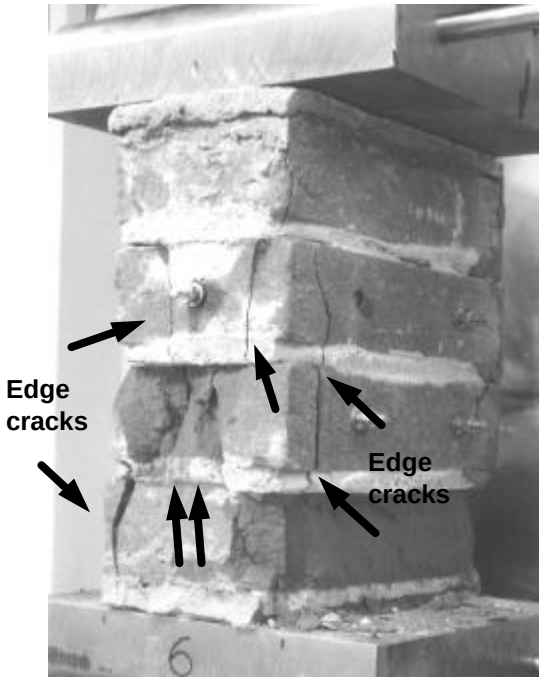

Figure 8 – Concentric loading – side D/C: internal cracking after removal of the detached parts. The double arrows indicate an internal core less damaged than the external part. Some evidences of external peeling

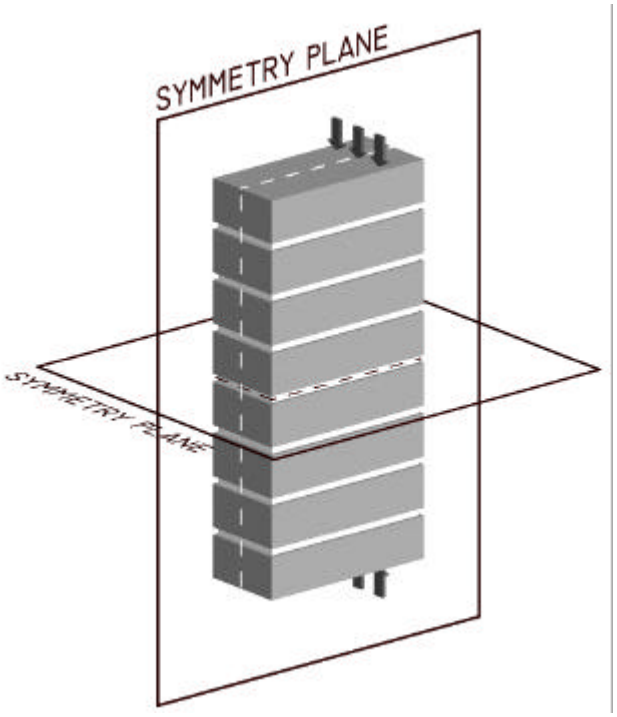

Figure 9 – a) Symmetry conditions and b) reduced model with symmetry restraints of an infinite stack of mortar joints and brick units

4. FEM MODELLING OF MASONRY

A FEM analysis of the mortar-brick stack should reproduce the stress distribution inside the brick. The symmetry conditions of an assemblage of mortar joints and bricks, Figure 9, allow to limit the analysis to be reduced to 1/4th of the joint/brick fundamental unit only (1/8th for concentric loading).

In the following, a non linear analysis up to collapse is performed assuming for the materials the values of Table 1. It has to be said that this choice may introduce some source of approximation since the material model in the FEM model is an isotropic one, while the experimental values are obtained from small specimens that may be significantly altered by local inhomogeneities. Nevertheless, test data were quite homogeneous, showing that inhomogeneities had no significant effect on the average. This latter consideration gives grounds to the assumption of an homogeneous material for mortar and fired clay.

The failure rule for the material, both mortar and brick, is the Willam-Warnke three-parameters model [17]. Figure 10 shows the failure surface in the deviatoric plane and on the tensile and compressive meridians. In order to represent the strong stress gradients, the mesh is quite dense (approx. 34.000 dof.s for 1/8th of the brick/mortar assemblage, average F.E. dimension equal to 3 mm). The procedure has been implemented in the ANSYS 5.7 code.

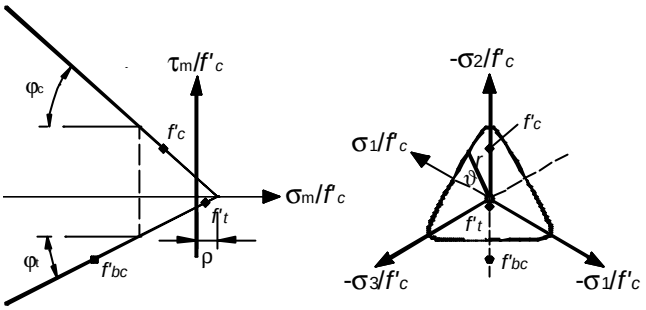

Figure 10 – Failure surface for the three-parameter Willam-Warnke model [17] a) on the tensile and compressive octaedric plane and b) on the deviatoric one; $f'_t = f'_c/10$ and $f'_{bc} = 1.3*f'_c$ (f'_{bc}: biaxial compressive strength)

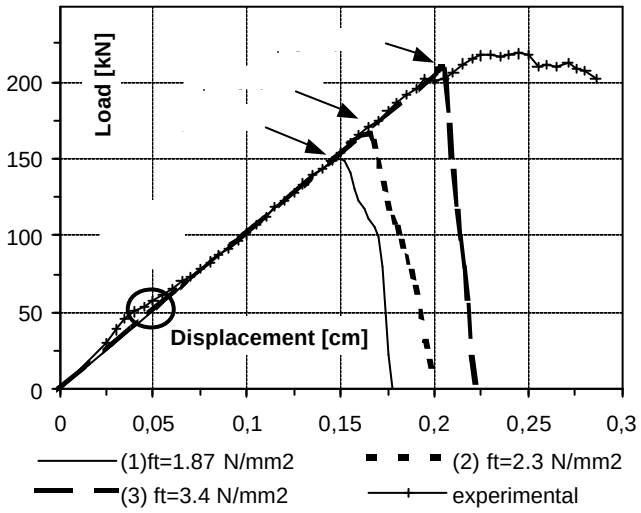

Figure 11 – Load/displacement curves for the theoretical model with different eccentricities of the load (displacement for a 270 mm long stack)

Since there is experimental evidence that no sliding takes place at the mortar/brick interface, probably due to the high compressive vertical stresses, the brick/mortar interface is allowed only to open when subjected to tensile stresses.

4.1 Concentric loading

Figure 11 shows the load/displacement response of the FEM model for an assemblage of mortar joints and bricks for different values of the brick tensile strength, along with the measured experimental data. The ratio between the tensile/compressive strength of the brick is rather high, 1/5.5≅0.18, so that lower values of the brick tensile strength were used in order to verify the applicability of the TPB test-deduced tensile strength to this kind of FEM models.

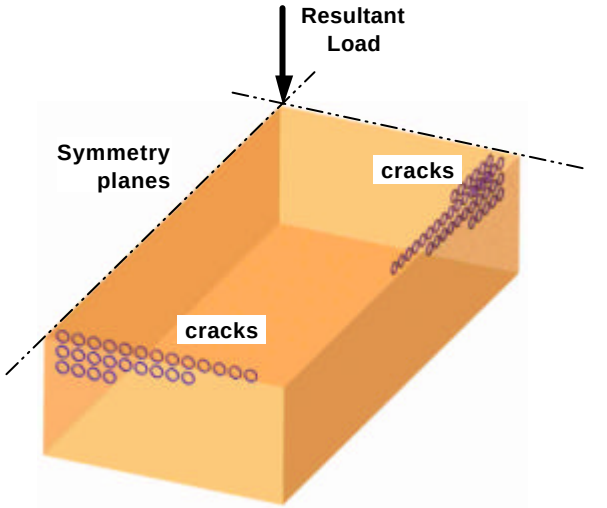

Figure 12 – Crack distribution in upper part of the brick in the neighbourhoods of the free edges at the very beginning of crack propagation

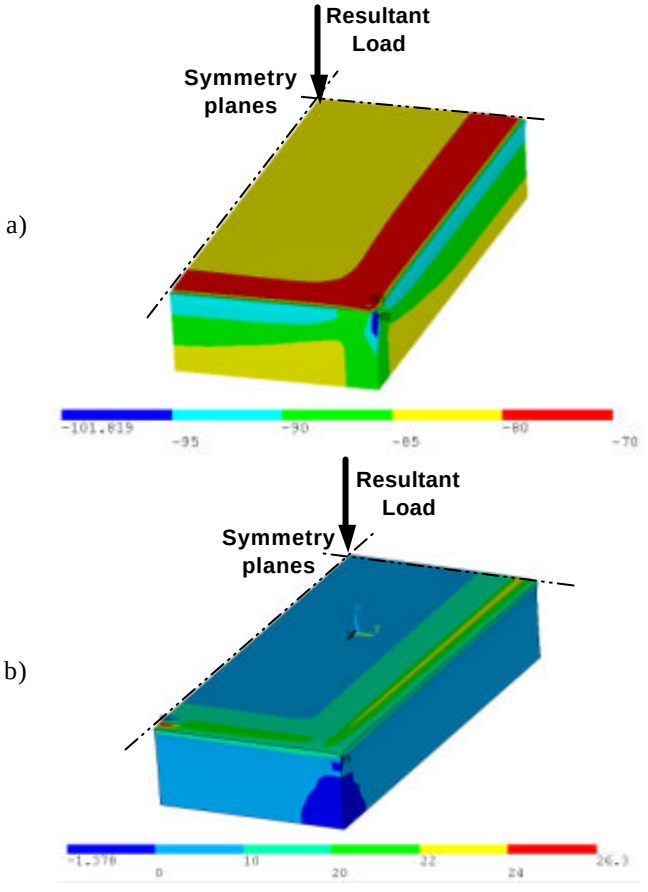

Figure 13 –Distribution of the a) vertical and b) principal tensile stresses at the initiation of the first cracks [N/mm^2 *10]. Upper part of the brick

The perfect agreement in the elastic phase should not be considered of great significance because the mortar elastic moduli, deduced via equation (1), is exactly the value which fits the global average elastic moduli of the prism. Much more interesting is the fact that the agreement with the elastic theory is still good up to more than 90% of the collapse load. The arrows indicate the point of the load history of each model at which cracking was activated in the FEM model. If we assume the acoustic emission as a proof of the activation of cracking, a significant difference from the experimental evidence has to be recognized. Since the acoustic emission is followed by a still linear response, it is not clear whether the early cracking is due to some specific experimental settlement or is a typical feature of masonry collapse.

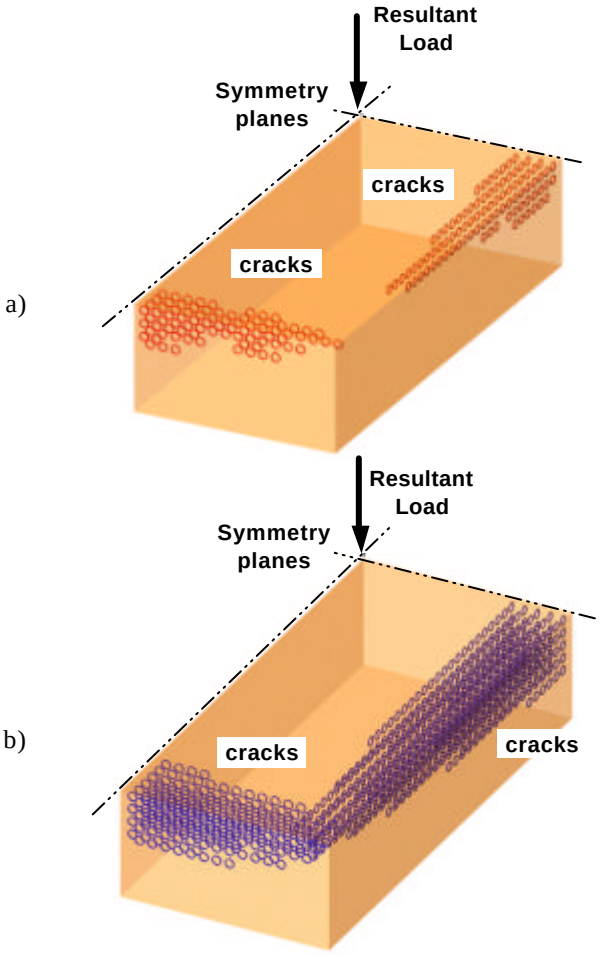

Figure 14 – Evolution of cracking at the very last stage of the loading process: a) 96%; b) 98% of the limit load. Upper part of the brick

The limit load reached by the FEM model with a 3.4 N/mm^2 tensile strength, the value measured in the TPB test, is very close to experimental value. The major difference is in the post-peak phase: FEM models foresee a catastrophic collapse, while the experimental evidence shows a limited but clear softening phase. As it has been observed, cracking activates close to the external surfaces and concentrates in a rather limited volume; in this way, the FEM models loose convergence as a consequence of locally concentrated cracks and are not able of representing the structural response when cracking spread throughout a

large part of the brick.

At the very beginning of crack propagation, the first crack appears at the brick/mortar interface, on the brick side only, in the neighbourhood (5-10mm) of the external free edges and parallel to the brick sides starting from the interface and directed towards the centre of the brick, Figure 12 - light grey lines. In spite of a quite uniform distribution in the brick of the vertical compressive stresses, Figure 13.a, accounting for a 8-8.5 N/mm^2 in the central area, in the area where the cracks activate, i.e. close to the free edges, a high tensile stress in attained, Figure 13.b, and reduced compressive stresses of 7-8 N/mm^2 are found, Figure 13.a. Such a limited crack damage is not enough to show a macroscopic non linear behaviour.

Collapse is attained when cracking passes through the brick thickness and spreads throughout the interface, with a sudden drop in the load carrying capacity of the brick/mortar assemblage. Substantially, collapse is a local phenomenon close to the free surfaces, as already conjectured by Rots [15].

Figure 14 shows the quick evolution of cracking in the brick, the mortar joint remaining undamaged till the limit point: cracks propagate both in length and in depth. The coalescence of the cracks makes a continuum damaged path to form on a surface approximately parallel to the free edge. This prevision is rather similar to the experimental evidence, Figures 7 and 8.

Worthwhile noting is the tensile stress distribution inside the brick, that turns out to be uniform only in the internal core of the brick, with stress concentration localised close to the free edges. If we assume the central part of the brick (with uniform tensile stress distribution) as the load carrying structure, we can reproduce the inner core of the prism, Figure 8. But this fact rises some doubts concerning the uniform tensile stress distribution in the brick assumed by many mechanical models, the limit-analysis based models [3-7].

4.2 Eccentric loading

The eccentric loading has been modelled for an eccentricity of 6 cm only, e/h = 0.27, allowing the brick/mortar interface to open but not to slide. The macroscopic response of the model is similar to that represented in Figure 11, with a long linear response up to 95% of the limit load and a sudden collapse at a total load of 82.4 kN, very close to the experimental value of 78.8 kN. The major difference arise in the structural response: the real specimen showed a clear non linear response from the early stages of the loading history, while the FEM model remains linear elastic till almost the limit load.

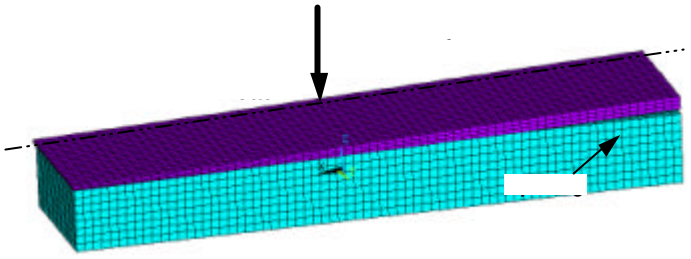

Figure 15 – Deformed shape of the masonry unit at 95% of the collapse load for a 6 cm eccentric loading

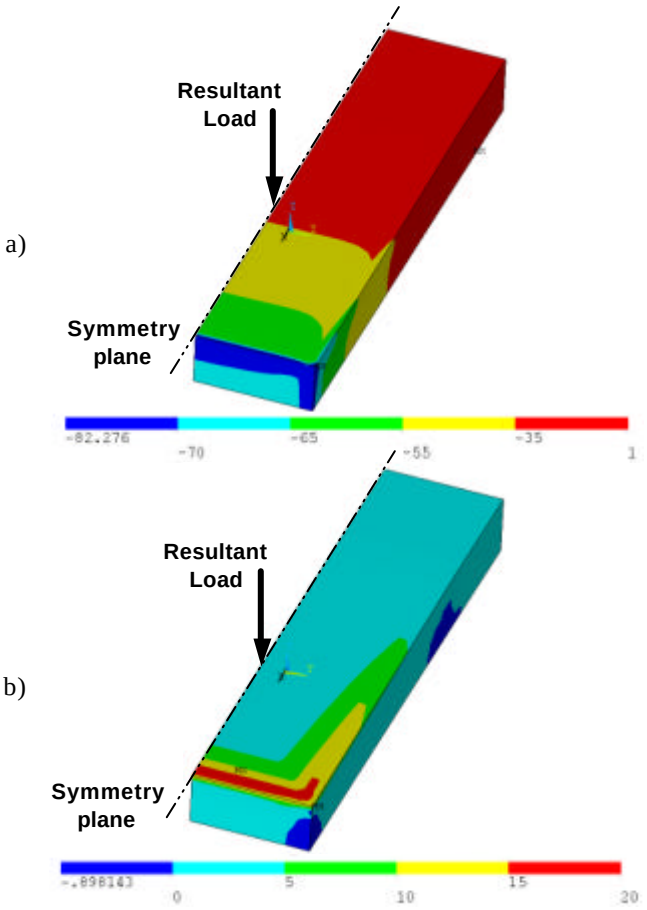

Figure 16 – a) Vertical and b) maximum tensile stress distribution at 95% of the collapse load [N/mm^2 *10]. Upper part of the brick

Also in this case the mortar joint remained undamaged till the limit point. Figure 12 plots the vertical and maximum tensile stresses just before the opening of the first cracks. Two observations arise: 1) the lines with equal vertical stress, Figure 12.a, are not straight with irregularity close to the free side, indicating that the neutral axis, straight on the average, suffers from local stress concentrations close to the edges; 2) close to the free side of the compressed part of the section high tensile stresses are developed. Exactly in that part the first cracks are developed starting from the symmetry axis, Figure 17.

On the brick/mortar interface the shear stresses that are developed are quite low, never more than 0.4 N/mm^2, Figure 18, with an average compressive stress of 6 N/mm^2; Whatever the friction coefficient at the interface, such low values of the tangential stresses justify the experimental evidence that no sliding occurs between the brick and the mortar joint.

These circumstances are only a first glance in the collapse mechanism of masonry prisms under non-uniform compressive stresses. More research is still needed, along with other experimental results.

5. COMPARISONS AND CONCLUSIONS

The experimental response of the specimen under uniform compression revealed to be rather linear up to some 90% of the limit load. Non-uniform compressive stresses with brick /mortar interface opening, instead, exhibit clear non linear

response starting from the very beginning of the loading process. Low load levels are needed to activate acoustic emission from the specimen; at the present stage of the research it is not clear whether this is due to bad workmanship of the specimen or it is some intrinsic feature of the collapse mechanism.

FEM models give e deeper insight in the cracking phenomenon. Cracks originate at the brick /mortar interface as a consequence of the elastic mismatch between brick and mortar, starting on the brick side of the interface and propagating towards the brick centre. This evolution of the crack pattern is in agreement with Rots [15] who conjectured that the collapse mechanism is activated by some local edge effect rather than a global failure condition in the brick core.

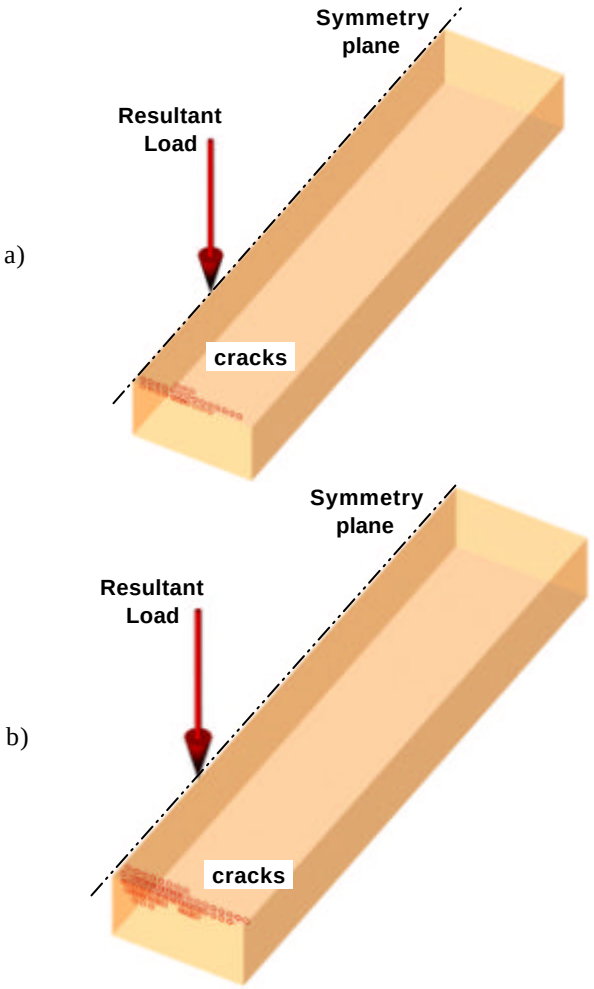

Figure 17 – Crack distribution at a) 95%; b) 98% of the limit load. Upper part of the brick

Besides, the crack pattern, the crack position and the corresponding load level reproduced by the FEM model seem to be in reasonable agreement with experimental evidence. If the mechanical properties of the materials are evaluated by means of standard testing procedures the limit load foreseen by the FEM model is reasonably good. Nevertheless, the non linear response of the prisms has still to be investigated.

The stress distribution, specifically the presence of some areas where stress concentration is found, rises some objection to the classical limit-analysis theory. The brick tensile strength seems to be attained closed to the free edges of the brick while the internal core exp eriences still low tensile stresses. This fact has been found on thin specimen, so that this conclusion cannot be extended to very thick eccentrically loaded masonry.

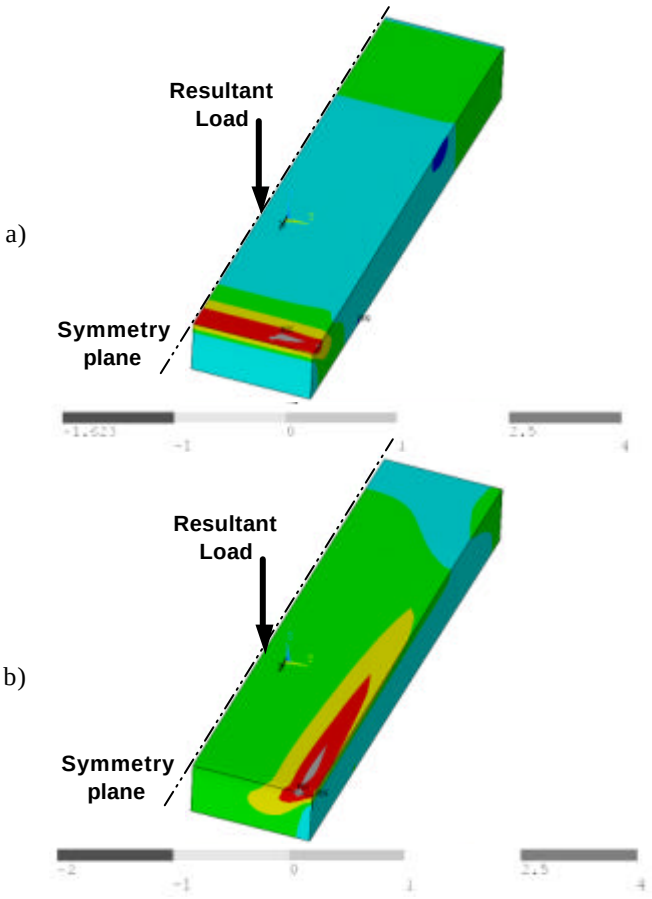

Figure 18 – Shear a) *xz* and b) *yz* (x is the direction of the longest side) at 98% of the collapse load [N/mm^2 *10]. Upper part of the brick

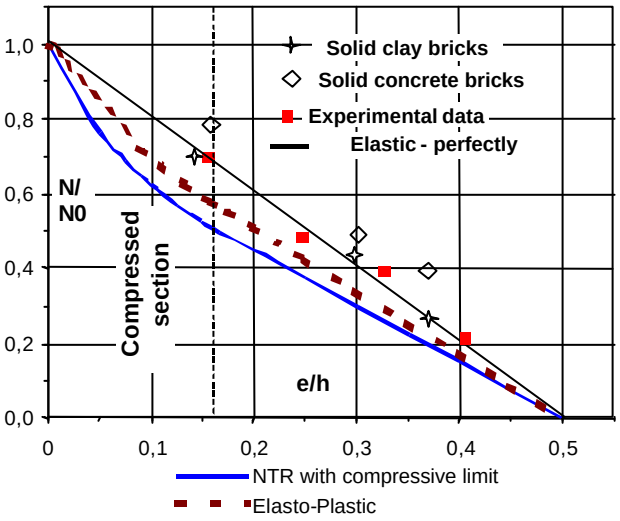

Figure 19 – Limit domain for eccentric loading assuming an NTR model with compressive stress limit and an Elasto-Plastic model with strain limit. Comparison with experimental data

Figure 19 plots the limit load measured in the tests against

the eccentricity, along with other experimental data [9, 18]. Three limit lines represent the limit load calculated according to different mechanical models. From the uniform loading test the actual compressive strength of the brickwork can be deduced along with the ultimate strain, Figure 4. Three different simple models lead to different failure loads: a) a pure No-Tensile-Resistant model in which a limit is set to the compressive stresses –bold solid line; b) an elastic-perfectly plastic model [19] to which the failure condition is reached when the maximum compressive strain attains the ultimate value measured in a concentric loading test – dashed bold line; c) an elastic-perfectly plastic model with unlimited ductility –thin solid line. More sophisticated models can be formulated but they would not add any further information at the present stage of the research.

The experimental data, except those for solid concrete brickwork, lie somewhere in-between the NTR and Elasto-Plastic with strain limit curves. This suggests that the effective response of masonry is something more than No-Tensile-Resistant. Even though the limited number of specimen does not allow a general conclusion, the experimental results showed that the assessment of an arch-type structure relying on a purely NTR model turns out to be significantly conservative. A more detailed approach could consider the development of limited inelastic strains inside masonry.

Many failure theories were used to foresee the compressive strength of masonry. Table 2 summarizes the estimates of the compressive strength according to some of these theories and to some codes employing the mechanical parameters of Table 1. For the code-type approach, it has to be said that codes give characteristic values of the strength, while the comparison should here be drawn relying on the average values, which are usually 20-30% higher. If the code values are multiplied by a factor 1.2-1.3, the experimental value is obtained.

Table 2
Estimated concentric compressive strength of masonry

Reference	Notes	Estimated compressive strength [N/mm^2]
Francis [3]	elastic theory	15.0
Hilsdorf [6]	limit analysis	13.7
Khoo & Hendry [7]	limit analysis + experimental	17.8
EC 6 [20]	-	7.4
Fiche-UIC [21]	-	7.8
Italian Code [22]	for M2 mortar	7.4
Italian Code [22]	for M3 mortar	6.8
Present work	experimental	9.9

The results of table 2 underline that the limit-analysis approach somehow overestimates the actual compressive strength of masonry, while modern codes, probably relying on a large base of experimental data, give empirical formulas which may fit quite well the experimental data. This is probably due to the fact that the materials used for the specimens were modern materials, the ones the empirical formulas had been developed for.

More research needs to be carried out in order to widen the experimental data and to get deeper insight in the mechanisms that activate after the maximum load is reached and lead to a significant softening phase of the non uniformly compressed specimen. This phenomenon gets poor detailing at the present level of the research.

AKNOWLEDGEMENTS

The authors acknowledge the contribution by Giancarlo Sighieri to the experimental work, mainly in solving the technical problems and in preparing the testing setup.

This research was carried out with the financial support of the (MURST) Department for University and Scientific and Technological Research in the frame of the PRIN 2002/ 2003 Project "*Safety and Control of Masonry Bridges*".

REFERENCES

1. HENDRY, A.W., *Structural Brickwork*, John Wiley, New York, 1981

2. DRYSDALE, R.G., HAMID, A.A., BAKER, L.R., *Masonry Structures, Behavior and Design*, Prentice Hall, Englewood Cliffs, 1993.

3. FRANCIS, A.J., HORMAN, C.B., JERREMS, L.E., The effect of joint thickness and other factors on the compressive strength of brickwork, *Proc. 2nd I. B. MA. C.*, Stoke on Kent, 1971.

4. ATKINSON, R.H., NOLAND, J.L., A proposed failure theory for brick masonry in compression, *Proc. of the 3rd Can. Mas. Symp.*, Edmonton, 1983.

5. SHRIVE, N.G., A fundamental approach to the fracture of masonry", *Proc. 3rd Can. Mas. Symp.*, Edmonton, 1983.

6. HILSDORF, H.K., Investigation into the failure mechanism of brick masonry under axial compression, in *Designing, Eng.ng & Construction with Masonry Products*, F.B. Johnson ed., Gulf Publishing, Houston, Texas, 1969.

7. KHOO, C.L., HENDRY, A.W., A failure criteria for brickwork in axial compression, *Proc. 3rd I. B. MA. C.*, Essen, 1973.

8. PAGE, A., BROOKS, D., Load bearing masonry – A review, in *Proc. of the 7th I. B. M. C.*, Melbourne, 1985.

9. DRYSDALE, R.G., HAMID, A.A., Effect of ec-centricity on the compressive strength of brickwork, *J.nl Brit. Cer. Soc.*, **30**, 1982.

10. MAURENBRECHER, A.H.P. Compressive strength of eccentrically loaded masonry prisms, *Proc. III Can. Mas. Symp.*, Edmonton, Canada, June 1983.

11. TAYLOR, N., MALLINDER, P. The brittle hinge in masonry arch mechanism, *Str. Eng.*, **71**, 1993.

12. BINDA, L., MIRABELLA ROBERTI, G., TIRA-BOSCHI, C., ABBANEO, S., Measuring masonry material properties, *Proc. U.S.-Italy Workshop on guidelines for seismic evaluation and rehabilitation of unreinforced masonry buildings*, section VI, 1994.

13. ATKINSON, R.H, NOLAND, J.L, ABRAMS, D.P. A deformation failure theory for stack bond prisms in

compression, *Proc. VII I.B.Ma.C.*, Melbourne, Aus., 1985.

14. RABIAIOLI R., Control methods for masonry arch bridges: an example (in italian), *Ing. Ferr.*, August 1993.

15. ROTS, J.G. Numerical simulation of cracking in structural masonry, *Heron*, **36**, 1991.

16. BRENCICH, A., GAMBAROTTA, L. Isotropic damage model with different tensile-compressive response for brittle materials, *Int. J.nl Sol. Str.*, **38**, 2001.

17. WILLAM, K., WARNKE, E. D., Constitutive model for the triaxial behaviour of concrete, Proc. IASBE, vol. 19, ISMES, Bergamo, 1975.

18. DRYSDALE, R.G., HAMID, A.A. Capacity of concrete block masonry prisms under eccentric compressive loading, *ACI J.nl*, **80**, June 1979.

19. BRENCICH, A., DE FRANCESCO, U., GAMBAROTTA, L. Elastic no tensile resistant – plastic analysis of masonry arch bridges as an extension of Castigliano's method, *Proc. 9th Can. Mas. Symp.*, Fredericton, 2001.

20. ENV 1996-1-1 march 1998 - EURO CODE 6. Design of masonry structures, Part 1-1: General rules for buildings – Rules for reinforced and un-reinforced masonry, 1998.

21. FICHE-UIC 778-3E. Recommandations pour l'evaluation de la capacite portante des ponts-voutes existants en maçonnerie et beton, 1994.

22. DEPARTMENT OF PUBLIC WORKS. Technical code for design, building and assessment of masonry buildings and their strengthening – 20th November 1987 (in Italian).

APPENDIX

Notation

$\sigma_x, \sigma_y, \sigma_z, \tau_{xy}, \tau_{xz}, \tau_{yz},$	components of the stress tensor
E_b, n_b	Elastic modulus and Posson's ratio for brick
E_m, n_m	Elastic modulus and Posson's ratio for mortar
E_M	Elastic modulus for masonry
f_c	uniaxial compressive strength
f_{bc}	biaxial compressive strength
f_t	uniaxial tensile strength
t_b	brick thickness
t_m	mortar joint thickness
h	brick length (maximum dimension)
e	load eccentricity
$h_b = t_b/(t_m + t_b)$	brick volume ratio
$h_m = t_m/(t_m + t_b)$	mortar volume ratio